JOURNAL OF AIRCRAFT
Vol. 44, No. 1, January–February 2007

Analysis of the Airframe Noise of an A320/A321 with a Parametric Method

Daniel Blacodon
ONERA/DSNA, 92322 Châtillon Cedex, France

DOI: 10.2514/1.20295

A spectral estimation method based on measurements by a phased array was developed to estimate absolute power levels radiated by compact or extended sources. After a brief recall of its principle, numerical simulations involving several source regions are presented to illustrate the accuracy and the high-resolution performances of this new method. Tests were carried out with a 1:11th scale A320/A321 Airbus model in the anechoic wind tunnel CEPRA 19. The characteristics of source regions from inboard to outboard of the wing slat and flap, and the main and nose landing gear subregions are examined. The dependence in level and frequency of the model subregions with the flow speed, the effects of the attack angle, and the effects of the flap or slat deployment are studied. The different trends revealed by the integrated power levels are also discussed. Examples of the localization of noise sources identified with conventional beam forming and the new method are presented. The consistency of the results is examined by comparing the integrated power levels for the complete wing and the measured spectra with the phased array. Finally, we show that the spectral estimation method is quite reliable in computing the far-field directivity of airframe noise sources.

I. Introduction

IT has been established that airframe noise is a significant contributor to the overall acoustic emissions of a civil aircraft at landing. The dominant sources of airframe noise are known to be associated with the high-lift devices and with the landing gear of the aircraft [1–5]. The reduction of aerodynamic noise is a priority for the civilian aeronautics industry, which in the next decade will be confronted with more restrictive noise regulation in urban flyover areas. A 1:11th scale A320/A321 Airbus model was tested in the CEPRA 19 anechoic wind tunnel by ONERA, within the framework of the European project for the reduction of airframe and installation noise (RAIN) [6] and under a contract from Airbus Industries and SPAé (French Service of Aeronautic Programs). The objective of this experiment was to identify and quantify the contribution of airframe noise sources to the overall noise radiated in far field. As in many acoustic studies carried out in a wind tunnel facility, the characterization of acoustic sources detailed in this paper is based on data provided by a phased array of microphones [7–10].

In the last decade, significant progress was made in the development and effective application of methods that give an estimate of the absolute levels of acoustic sources. Certain methods such as deconvolution [11] use an inverse technique to restore the sound power levels (SPL) of interest from the output of conventional beam forming (CBF). In contrast, the spectral estimation method (SEM) [12] implemented in this study is based on a direct estimation of the desired SPLs from the array cross-spectral matrix (CSM).

The first part of the paper is devoted to a short review of the problems occurring in the power level estimation of acoustic sources and to a discussion of several methods that have been suggested in the literature to solve this problem.

In order to verify that SEM is appropriate to correctly characterize airframe noise, which is broadband in nature, the accuracy of the results provided by this method at low, medium, and high frequencies is examined with numerical simulations in the second part of the paper.

The data analysis of airframe noise radiated by the aircraft model is presented in the third part of the paper. The consistency of the results provided by SEM is discussed in the last part of the paper.

II. Statement of the Problem: Inverse Solution

A scenario of compact and extended sources measured by an array of microphones is depicted in Fig. 1. The objective is to estimate the absolute levels generated by each source at their emission frequencies. One of the first techniques investigated to solve the power level estimation problem is the conventional beam-forming method. It has the advantage of being robust, easy to implement, and cheap in computation time. However, CBF is also known for having poor spatial resolution capabilities. Its ability to separate two closely spaced sources is linked to the beam pattern and more specifically to the width of the main lobe, the height of the side lobes, and the position of the first null at the output of the CBF. This method is appropriate for providing accurate estimates of the power levels of compact sources that are separated by more than a $\Delta_{3\,\mathrm{dB}}$ beamwidth (which is proportional to the wavelength of the acoustic sources and inversely proportional to the length of the array). In numerous applications, the acoustic sources are extended and CBF provides an overestimation of the expected power levels due to an overlapping of the beam patterns. One way to solve this problem is to improve the resolution capability of CBF by increasing the spatial aperture of the array. However, this technological solution is limited in practice, as it requires increasing the physical size of the array.

The problem encountered with CBF is similar to the one present in the computation of a spectrum from successive data blocks. The use of data measured by an array of finite length implicitly assumes the unmeasured data to be zero, which is usually not the case. This multiplication of the actual data by a window function means that the overall spatial transform (i.e., CBF) can be considered as the "convolution" of the actual source characteristics with the point spread function of the array manifold (i.e., array response). Thus, it appears that a "deconvolution" process of the result computed with CBF, by the array response, may restore the power levels of the acoustic sources that would be observed in the absence of the array resolution effects. The numerical simulations and experimental applications presented in [11] have shown that the deconvolution approach for the mapping of acoustic sources (DAMAS) is appropriate for obtaining the true levels of the acoustic sources.

Presented as Paper 2809 at the 11th AIAA/CEAS Aeroacoustics Conference en Exhibit, Hyatt Regency Monterey, 23–25 May 2005; received 28 September 2005; revision received 7 March 2006; accepted for publication 31 March 2006.

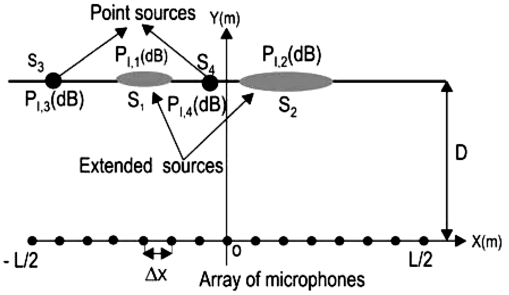

Fig. 1 Geometry of the problem of acoustic source SPLs estimation.

Moreover, in the case of extended source regions, the deconvolution method is associated with a spatial integration over the areas of interest, in order to restore their actual total power levels. However, performing deconvolution on the output of the CBF has several drawbacks. Indeed, some difficulties may occur in the estimation process if information concerning the acoustic sources of interest is masked by CBF at low frequencies or by undesirable phenomena (background noise, replica sources) present in the output of CBF at high frequencies.

A. SEM Method: Direct Solution

The so-called SEM method has been suggested in [12] to overcome the problems associated with the CBF, discussed in the previous section. The purpose here is to extract the levels of the acoustic sources directly from the observed CSM rather than using the output of the CBF, to avoid corruption of the source levels by the array pattern. The premise for the development of the method is based on the fact that the array CSM is an indirect measurement of the source power levels of interest. Hence, the problem here is to find the parameters (i.e., the power levels of the source areas) of the model matrix, with respect to the measured CSM. A standard approach in the estimation procedure consists of sampling source areas, such that at each sampling point there is a potential source for which the power level remains to be found. An iterative method for fitting the array CSM to the model one is used to determine the amplitudes of the point sources. We shall now detail the three steps necessary in the implementation of SEM.

B. Step 1: A Model for the CSM

In practical situations, it is not the details of noise sources such as the slats, the flaps, and the landing gears for an aircraft at landing that are needed, but their directivity pattern in the far field to assess their contribution to the overall noise radiated. However, the problem is complex if we want to extract from the phased array data the directivity pattern of different extended source regions radiating simultaneously. At this point, the concept of extended noise source measured through its radiation must be clarified to get a better understanding of the true nature of the problem that we want to solve. It is shown in [13] that the measurement of the acoustic field outside the source region is not sufficient to uniquely determine the characteristics of the source. This implies that an extended noise source may only be viewed as an equivalence class between source functions radiating the same pressure field on a phased array. A valuable equivalent source model could be a distribution of correlated monopoles, which allows the characterization of any directivity. However, the problem of finding both the amplitude of the sources and their correlation function in amplitude and phase involves a very large number of parameters, and it is not easy to solve with a limited number of microphones. In this study, a majority of noise sources have smooth directivity patterns. This means that if the aperture angle of an array of microphones seen from the overall source region is not too large, the directivity pattern of each region may be considered as isotropic within this aperture. However, in practice, one is free to process other apertures by moving the array or the sources. Therefore, a model based on a set of uncorrelated monopoles, like the one used in the paper, is quite appropriate to study airframe noise.

Accordingly, the model cross power spectrum $\Gamma^{\mathrm{mod}}_{m,n}(f)$, between the output signals of the mth and nth microphones, can be expressed as follows:

$$\Gamma^{\mathrm{mod}}_{m,n}(f) = \sum_{i=1}^{J} G_{m,i} A_i(f) G^*_{n,i} \tag{1}$$

J is the number of monopole sources considered for the description of all acoustic subregions, $G_{m,i} = e^{jkR_{mi}}/R_{mi}$, R_{mi} represents the distance between the ith monopole and the mth microphone, $A_i(f)$ indicates the power level of the ith monopole to be estimated, and the superscript $*$ stands for the complex conjugation.

C. Step 2: Estimation of the Parameters

The computation procedure consists of determining the power levels A_i of the virtual uncorrelated monopoles, by minimizing the error between the array $[\Gamma^{\mathrm{mes}}_{m,n}(f)]$ and the model $[\Gamma^{\mathrm{mod}}_{m,n}(f)]$ cross-spectral matrices given by

$$F(A) = \sum_{m,n=1}^{M} \left| \Gamma^{\mathrm{mes}}_{m,n} - \sum_{i=1}^{J} G_{m,i} A_i G^*_{n,i} \right|^2 \tag{2}$$

However, solutions A_i obtained after the minimization process [Eq. (2)] are not guaranteed to be positive. This can lead to physically unrealistic solutions for the recovered spectra (i.e., spectra with negative amplitudes). Adding a positivity constraint on parameters A_i by using the following relation can easily circumvent this drawback:

$$F(A) = \sum_{m,n=1}^{M} \left| \Gamma^{\mathrm{mes}}_{m,n} - \sum_{i=1}^{J} G_{m,i} A_i G^*_{n,i} \right|^2 \tag{3}$$

subject to $A_i \geq 0$.

It is worth pointing out that the inverse methods for solving the least square problem under a nonlinear constraint [Eq. (3)] may be difficult, or indeed impossible to implement. An alternative approach to obtain the parameters of interest consists of using an iterative technique, which verifies that the positivity constraint on parameters A_i is satisfied at each iteration. Unfortunately, this class of iterative methods is generally much more costly in computational time than methods, which solve unconstraint problems. This difficulty can be eliminated by replacing parameters A_i in Eq. (3) by a new set of parameters such as $\alpha_j^2(f) = A_i(f)$, which implicitly contain the constraint of positivity. After this step, one obtains a problem without constraint of the following form:

$$F(\alpha) = \sum_{m,n=1}^{M} \left| \Gamma^{\mathrm{mes}}_{m,n} - \sum_{j=1}^{J} G_{m,j} \alpha_j^2 G^*_{n,j} \right|^2 \tag{4}$$

In this study, parameters α_j^2 in Eq. (4) are estimated with a conjugate gradient method [14] which has the major advantage of a fast convergence rate. This point has been verified here since the results detailed in the following sections were all obtained after only 400 iterations.

D. Step 3: Subregions Power Levels

In practice, N_q uncorrelated monopole sources are used to describe each acoustic source region of interest S_q. Accordingly, the integrated power level $P_{I,q}(f)$ output of the subregion S_q is simply obtained by incoherently adding the parameters α_j^2 found by the minimization process of Eq. (4), using the following relation:

$$P_{I,q}(f) = 10 \log \frac{\sum_{j=1}^{N_q} \alpha_j^2(f)}{p_0^2} \tag{5}$$

where $p_0 = 20\ \mu$Pa.

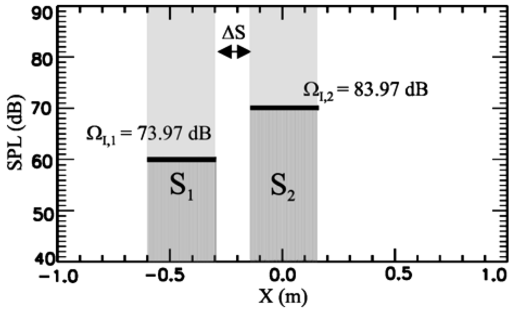

Fig. 2 Simulation of two extended sources S_1 and S_2 with unequal power levels separated by ΔS.

III. Simulation Results

The purpose of this section is to evaluate the ability of SEM to successfully estimate levels of extended acoustic sources that radiate broadband noise simultaneously as this can occur in practical situations. One considers two extended sources S_1 and S_2, with unequal power levels (Fig. 2). The sources S_1 and S_2 are composed of 25 uncorrelated monopoles evenly spaced of $\Delta_s = 0.005$ m. The levels of each monopole source for S_1 and S_2 are, respectively, $10\log A_1 = 60$ dB and $10\log A_2 = 70$ dB. Hence, by taking into account the assumption of uncorrelated monopole sources, the integrated power level $\Omega_{I,1}$ for S_1 may be obtained with the following relation:

$$\Omega_{I,1} = 10\log\sum_{n=1}^{25} A_1 = 73.97 \text{ dB} \tag{6}$$

By substituting A_2 into A_1 in Eq. (6), we find that the integrated power level for S_2 is equal to $\Omega_{I,2} = 83.97$.

The separation Δ_s between two consecutive monopole sources is defined as much smaller than a standard beamwidth $\Delta_{3\,\mathrm{dB}}$ ($\Delta_s < \Delta_{3\,\mathrm{dB}}/10$, $\Delta_{3\,\mathrm{dB}} \approx 1.22\lambda D/L$, $\lambda = f/c$, c denotes the speed of sound in the medium of propagation), so that S_1 and S_2 can be considered as continuously distributed.

The wave field generated by the two sources is assumed to be measured by a linear array of length $L = 1.4$ m, with $M = 15$ microphones separated by 0.1 m (Fig. 1). The distance between the array and the line source is $D = 2$ m. With this configuration, CBF can resolve, up to 6 kHz, the two sources S_1 and S_2 separated by at least a $\Delta_{3\,\mathrm{dB}}$ beamwidth. Above 6 kHz, it has been shown in numerical simulations not presented here, that the output of CBF is corrupted by aliasing phenomena characterized by grating lobes with peak levels equal to that of the main beam. An illustration of this undesirable phenomenon is considered in scenario 3 of this section.

A. Scenario 1: Computation at Low Frequency

The result given by CBF at the emission frequency of 600 Hz for the two extended sources S_1 and S_2 shows that the weaker source S_1 is masked by the side lobes of the dominant source S_2 (upper plot in Fig. 3). This result was foreseeable because the spatial separation ΔS between the two sources is $0.15\Delta_{3\,\mathrm{dB}}$, which is less than the minimum separation required for their resolution. The integrated power level computed with the output of CBF is $\tilde{P}_{I,1} = 97.25$ dB for the weaker source region S_1, and $\tilde{P}_{I,2} = 101.49$ dB for the dominant source region S_2. There is an overestimation of at least 18 dB of the actual power levels of S_1 and S_2.

The result presented in Fig. 3 (lower plot) indicates that SEM works correctly at the low frequency of 600 Hz for which the sources S_1 and S_2 are spatially separated by a fraction of $\Delta_{3\,\mathrm{dB}}$ ($\Delta S = 0.15\Delta_{3\,\mathrm{dB}}$). S_1 and S_2 are not completely resolved but their integrated levels are estimated within 0.8 dB of the actual values.

This first result illustrates how CBF introduces errors on the amplitude of the two source distributions due to the self-convolution between the sources S_1 and S_2 and the array response for these extended sources. In contrast, SEM gives accurate results, because it directly extracts the source characteristics from the array CSM that is not corrupted by array response.

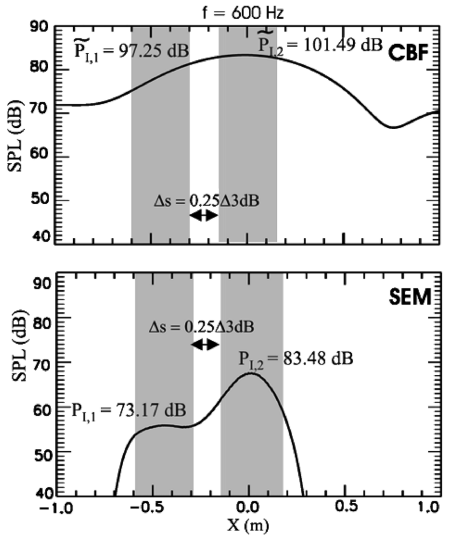

Fig. 3 Scenario 1: S_1 and S_2 are separated by less than a $\Delta_{3\,\mathrm{dB}}$ bandwidth at their emission frequency of 600 Hz. Results obtained with CBF and SEM.

B. Scenario 2: Computation at Midfrequency

In this example, the two acoustic sources S_1 and S_2 are separated by a $\Delta_{3\,\mathrm{dB}}$ beamdwidth at an emission frequency of 4 kHz. Clearly, CBF is able to resolve the two source regions (upper plot in Fig. 4). Although, this situation is favorable for CBF, the disagreement between the actual and estimated integrated power levels is again significant here. It reaches 14 dB for the weaker source region S_1, while it is 13 dB for the dominant source region S_2.

The result given by SEM is plotted in Fig. 4 (lower plot). We can note that S_1 and S_2 are well separated and the differences between the actual and estimate power levels of the two sources do not exceed 0.2 dB.

C. Scenario 3: Computation at High Frequency

In the last scenario, the two sources S_1 and S_2 are assumed to emit at 10 kHz. At this frequency the $\Delta_{3\,\mathrm{dB}}$ criterion is well satisfied because the separation between S_1 and S_2 is of $2.53\Delta_{3\,\mathrm{dB}}$. However, there is ambiguity in identifying the location of the two sources with CBF in Fig. 5 (upper plot). Indeed, there are three dominant sources

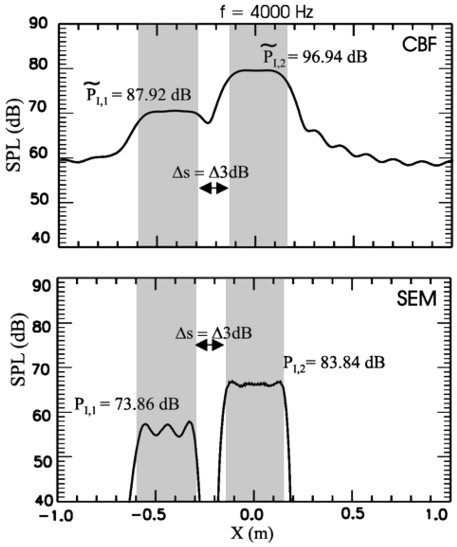

Fig. 4 Scenario 2: S_1 and S_2 are separated by a $\Delta_{3\,\mathrm{dB}}$ beamwidth at 4 kHz. Results provided by CBF and SEM.

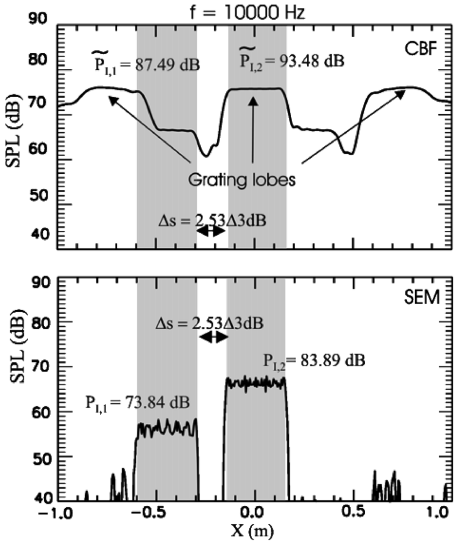

Fig. 5 Scenario 3: S_1 and S_2 are separated by more than a $\Delta_{3\,dB}$ beamwidth at 10 kHz. Results given by CBF and SEM.

with the same level. There is one source at the location of S_2 surrounded by two spurious sources (i.e., grating lobes). These are generated by the aliasing phenomenon because the array has been used at a frequency of 10 kHz, much greater than 6 kHz, the maximum frequency for which it was designed. Moreover, as in the previous example, the overestimation of the integrated power levels of the two source regions reaches 13 dB.

The result provided by SEM (lower plot in Fig. 5) is not subject to aliasing phenomenon at 10 kHz because its output does not derive from a spatial transformation of the array CSM, as is the case for the result given by CBF. Moreover, the two source regions S_1 and S_2 are resolved and their integrated power levels correctly estimated.

This last example clearly illustrates the fact that direct methods have a major advantage compared to inverse methods, because they can provide accurate results up to frequencies which are much higher than the frequency limit fixed by array geometry.

IV. Experiment Setup and Data Analysis

CBF and SEM are applied in this section to the tests carried out with a 1:11th scale A320/A321 Airbus model of Airbus Industries, in the CEPRA 19 anechoic wind tunnel (Fig. 6). It was equipped with a nozzle of three meters in diameter making wind velocities up to 60 m/s possible. A schematic drawing (Fig. 7) exhibits the test section with the aircraft model, the cross-shaped phased array, and far-field microphones used for acoustic measurements. The phased array is composed of two sub cross-shaped arrays with 40 half-inch microphones AKSUD 3211 (Fig. 8). The large array with a spatial aperture of 1.4 m × 1.4 m and the small array with an aperture of 0.6 m × 0.6 m have been designed to work at low and high

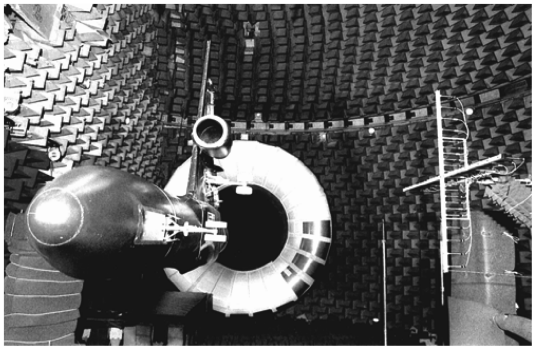

Fig. 6 Detailed view of the test setup in CEPRA 19 with the A320/A321 aircraft model.

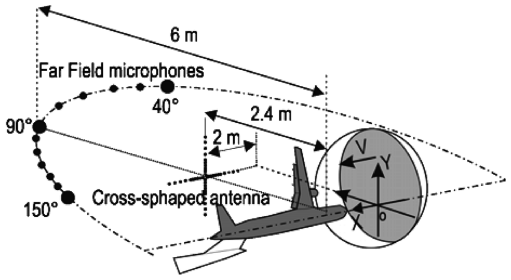

Fig. 7 Locations of far field and phased array microphones.

frequencies, respectively, with good resolution capabilities. However, the array responses present cross sides-shaped side lobes with high levels that reflect the geometry of array. It is obvious that this drawback is a major limitation in the characterization of acoustic sources with CBF. In this paper, reduction of the side lobes level is obtained by using an optimum signal processing method suggested by Élias [7], which artificially increases the number N of microphones of the cross-shaped array to obtain an array response similar to the one of a planar array of N-by-N microphones.

The far-field microphones are 12 $\frac{1}{4}$-inch Bruel & Kjaer (4135), located on a circular arc with an aperture of 110 deg (from 40 deg up to 150 deg) and a radius of six meters. A calibration of the array and far-field microphones was carried out before each test with a piston phone. The array matrix $[\Gamma^{mes}]$ needed for CBF and SEM was estimated using 200 data blocks including 1024 samples at the sampling frequency f_s. To avoid high background noise induced by the flow on the microphones, the array was positioned out of the flow at a distance of 2.4 m from the longitudinal axis of the aircraft model. Consequently, the correction of refraction and convection effects of the acoustic rays between the focus points on the aircraft model and the microphones of the array are taken into account [15,16] in the model CSM to obtain actual locations and levels of the acoustic sources. The localization maps were computed almost in real time with CBF over a grid of 2011 focus points separated by a distance of 0.04 m. The integrated power levels of the acoustic source regions were obtained with SEM from a postprocessing of the recorded array CSM because the method was not available during the tests that took place in 1999.

A. SEM Validation Using the CBF Result

Before discussing the data analysis, we present an illustration of the capability of SEM in the power level estimation of two-dimensional sources, similar to those encountered in practice. The idea here is to start from a localization result obtained by CBF during the tests carried out with the aircraft model A320/A321 (Fig. 9a), then to attribute virtual levels at each of the five dominant source regions, and finally to try to restore these virtual amplitudes using

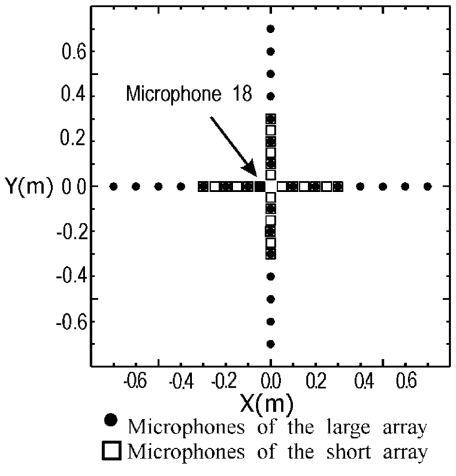

Fig. 8 Geometry of the phased array.

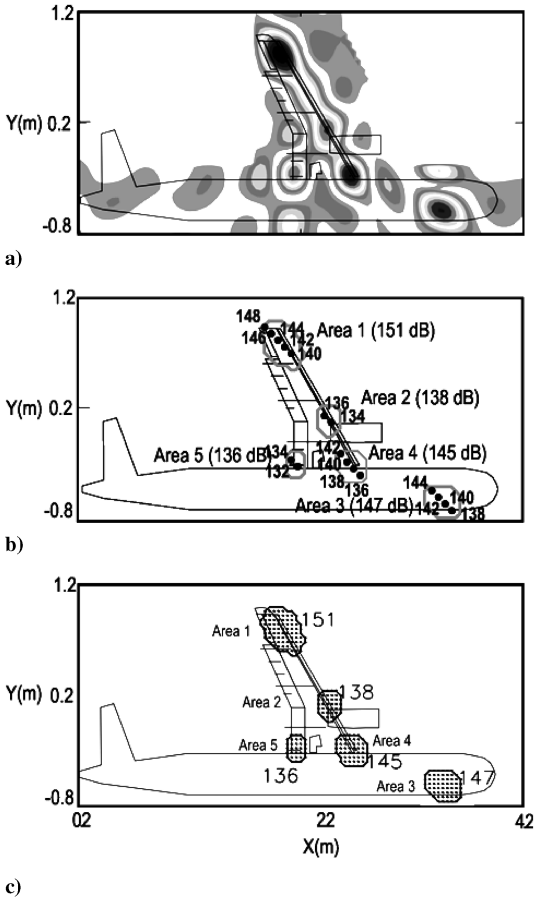

Fig. 9 a) Localization map computed with CBF; b) source areas and monopole amplitudes used for the simulation; and c) spatial sampling of the source areas and integrated power levels calculated by SEM.

SEM. For this purpose, one first extracts the contour of the main source regions from the output of CBF (Fig. 9b) using a procedure of image segmentation developed during this study. Then, up to five uncorrelated monopole sources are included in each of the contours to simulate extended sources. The locations of the monopole sources, their power levels, which are arbitrary and the integrated power levels of the five source regions in the range (136 dB, 151 dB) are shown in Fig. 9b. Figure 9c presents the sampling grid used for the test and the integrated power levels estimated by SEM. The good match between the actual power levels and their estimates shows that SEM is quite appropriate for the characterization of two-dimensional source regions similar to those that will be examined in the next section.

B. Data Analysis

The aim of the data analysis presented below is to assess the contribution to noise of each of the ten source regions (Fig. 10) identified as significant noise sources with CBF in a previous study, and for which it was not possible to associate true power levels until now. The sampling grid used by SEM to compute the output levels of the ten source regions is presented in Fig. 11.

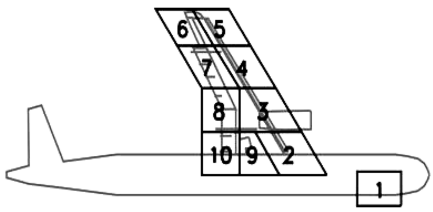

Fig. 10 Ten source areas considered in the study of airframe noise of the 1:11th scale A320/A321 Airbus model with SEM.

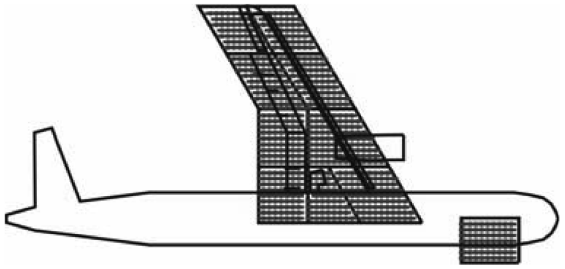

Fig. 11 Spatial sampling of the 10 source areas presented in Fig. 10.

The overall measured spectrum up to the frequency $f_{\max} = f_s/2$, with microphone 18 at the center of the array (Fig. 8) is compared to the integrated power levels of the ten source regions S_q $(q = 1, 2, \ldots, 10)$ computed with the SEM using the following relation:

$$P_{n=18}(f, q) = 10 \log \frac{\sum_{j=1}^{N_q} [\alpha_j^2(f)/R_{nj}^2]}{p_0^2} \tag{7}$$

The devices relevant to the discussion are the main landing gears (MLG), the nose landing gear (NLG) that can be up (U) or down (D), and the high lift devices (HLD). The main parameters considered during the experiments are the deflection angles S and F, respectively, of the slats and of the flaps, the angle of attack I of the model, and the wind tunnel flow velocity V.

1. *Effect of High Lift Devices*

Flap noise $S = 0° - F = 25°$: One first considers a configuration where only the flaps are deployed with an angle of 25 deg. In this example, the landing gears are retracted, the angle of attack is $I = 6$ deg, and the flow velocity is $V = 60$ m/s.

The measured spectrum plotted in Fig. 12 versus normalized frequencies $f/f_{\max}$ mainly shows a narrowband noise at low frequencies and a broadband noise, which decreases with the frequency.

The results obtained with SEM in Fig. 12 show, as it was foreseeable, that the level of noise generated by the slats is lower than that radiated by the flaps. The midboard of the flaps (region 8) significantly contributes to the increase of overall noise measured at low frequencies. There is a high-frequency tone noise radiated by the inboard flaps (region 10) at $f = 0.62\ f_{\max}$. However, it does not emerge significantly in the measured spectrum.

The results of localization computed with CBF and SEM at low frequency $f = 0.12\ f_{\max}$ are presented in Fig. 13. CBF exhibits a very broad dominant source and false noise sources, corresponding to the side lobes of the array response. These prevent us from

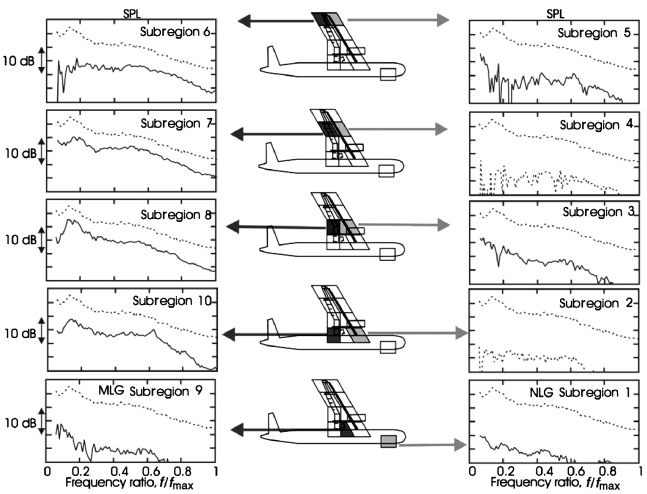

Fig. 12 Effects of HLD: $S/F = 0$ deg /25 deg. Measured spectra are the dashed lines and the SEM estimated spectra the solid lines.

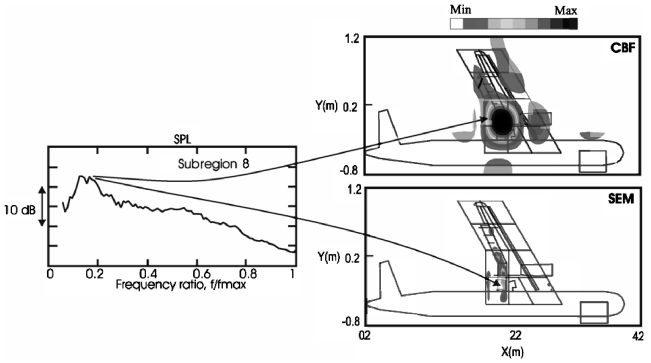

Fig. 13 Effect of HLD: $S/F = 0$ deg /25 deg. Localization maps are obtained with CBF and SEM and ranking of the noise sources at low frequency.

observing the correct distribution of acoustic sources. In contrast, we can see with SEM that noise sources are located at the leading edge of the flap inboard and midboard. This demonstrates how the high spatial resolution of the results provided by SEM can improve the knowledge of mechanisms generating airframe noise.

We also carried out the localization at the frequency of the tone noise $f = 0.62\ f_{\max}$. CBF gives a rough location of the tone source and again the side lobes of the array response (Fig. 14) whereas SEM provides the location of the tone source precisely. It is at the leading edge of the inboard tip of the flap.

$S = 27°$ and $F = 25°$: The deflection angle of the slats is fixed here at 27 deg. Other parameters of the previous test are left unchanged. The spectrum measured by microphone 18 of the array (Fig. 15, dashed line) exhibits at low frequencies:

1) a dominant narrowband noise centered at a frequency slightly higher than the narrowband noise observed in Fig. 12 when only the flaps were deployed, and

2) a strong tone noise at $0.25\ f_{\max}$.

The results given by SEM indicate that the dominant noise sources originate from the slats (Fig. 15). It appears, in particular, that the outboard (region 5), and the midboard of the slats (region 3) including the nacelle, significantly contribute to the overall noise radiated at low frequencies. The junction between the wing and the fuselage is also a strong noise source at low frequencies. One can see that the tone noise produced inboard on the flaps, at $f = 0.62\ f_{\max}$, in the configuration with the values of angles $S = 0$ deg and $F = 25$ deg, is completely masked by the acoustic sources generated by the slats.

2. *Effect of Flow Velocity*

The effect of the flow velocity is examined here for flow speeds ranging from $V = 30$ m/s to 60 m/s. For this, the landing gears are retracted, the value of the pitch angle is $I = 6$ deg, and the slats and the flaps are deployed with angles $S = 27$ deg and $F = 25$ deg, respectively.

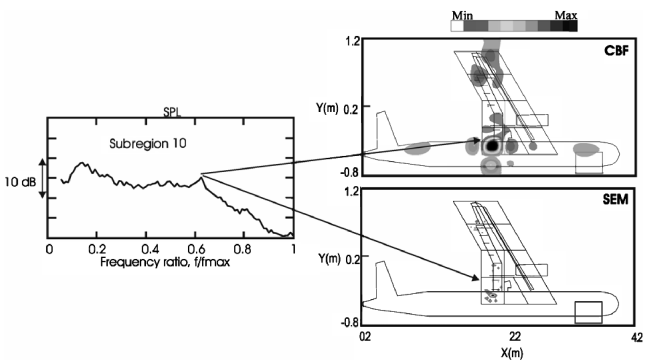

Fig. 14 Effect of HLD: $S/F = 0$ deg /25 deg. Localization maps are obtained with CBF and SEM and ranking of the noise sources at high frequency.

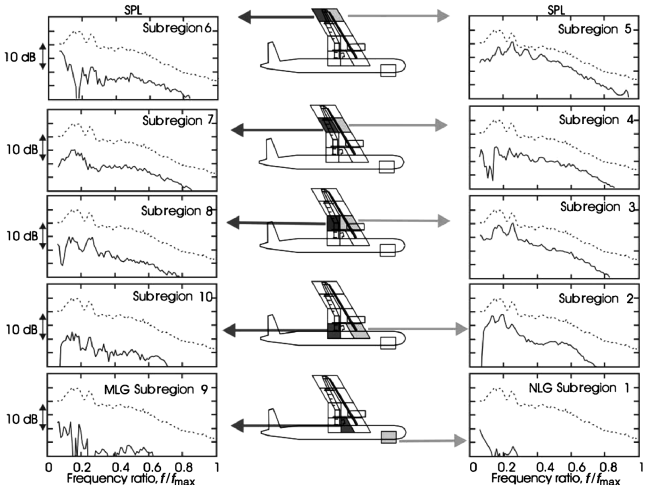

Fig. 15 Effects of HLD: $S/F = 27$ deg /25 deg. Measured spectra are the dashed lines and the SEM estimated spectra the solid lines.

The dependence with flow velocity of the noise levels radiated by the ten subregions clearly appears in Fig. 16. Indeed, these levels increase with the flow velocity. Furthermore, there are tone noises on the slats whose frequencies increase linearly with flow speed. However, this phenomenon is not observed on the flaps. The localization maps computed with SEM (Fig. 17) at low frequency for the highest flow velocity $V = 60$ m/s show that the tone noises are generated at the leading edge 1) of the inboard slats, at the junction between the wing and the fuselage, 2) of the midboard of the slats, just above the nacelle, and 3) of the outboard of the slats.

Following [2,3], we scaled the levels of the integrated spectra of regions 2, 3, 4, and 5 of the slats, 1 and 9 of the landing gears, and the region 6 outboard of the flaps with a speed law in $V^{6.3}$, and the regions 7, 8, and 10 of the flaps with a speed law in $V^{5.5}$. Now, the spectra collapse up to $f_{\max}$, except at the frequencies of the tone noise (Fig. 18). The tones, which are periodically spaced in each curve in Fig. 18, represent the harmonics of a fundamental frequency not identified in the measured spectra. We normalized the frequency using a Strouhal number $S_r = fA/V$ (A is a typical length) and scaled the spectra of subregions 2, 3, 5, and 10 with a speed law in $V^{5.5}$ in Fig. 19. It follows that the subregions 2, 3, 5, and 10 reveal identical tonal components, which collapse quite well at low frequencies.

3. *Effect of Angle of Attack*

In this last case, the SEM is applied for the three values of the angle of attack: $I = 4$, 6, and 8 deg. The value of the other parameters are

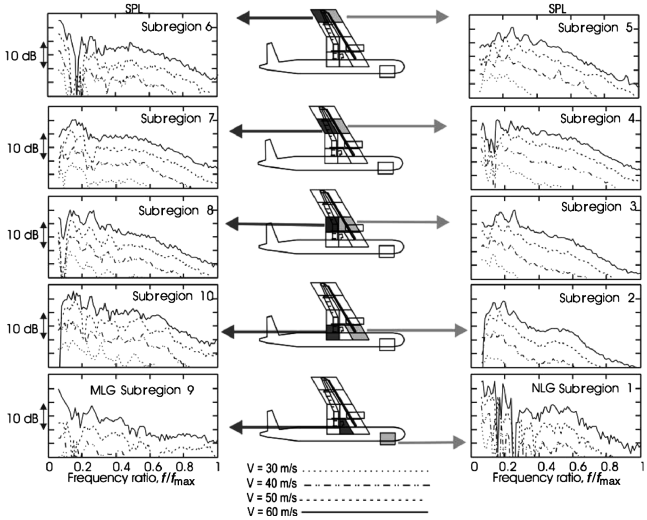

Fig. 16 Effects of the flow velocity.

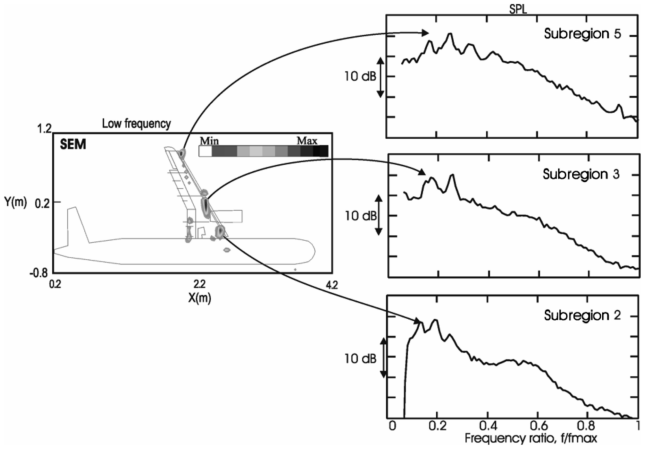

Fig. 17 Localization maps and ranking of the noise sources for $V = 60$ m/s obtained with SEM.

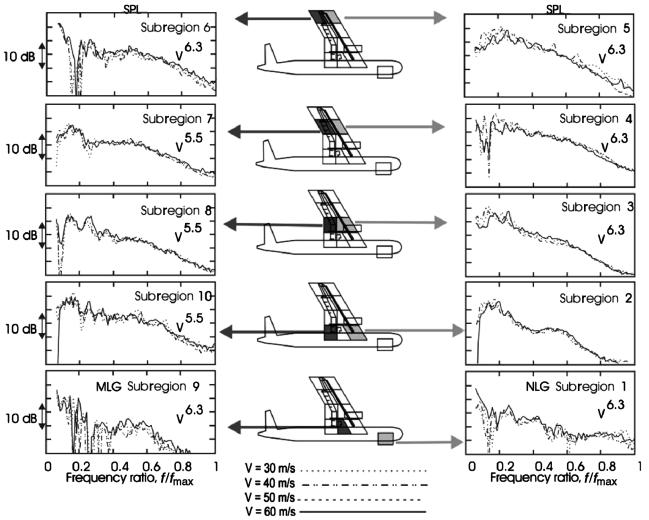

Fig. 18 Flow speed effects: scaled spectra with a speed law in V^{α}, $\alpha = 6.3$ for the subregions 1–6 and 9; $\alpha = 5.5$ for the subregions 7, 8, and 10.

$V = 60$ m/s, $S = 27$ deg, and $F = 25$ deg. The landing gears are deployed.

The upper plots in Fig. 20 show that the levels of the measured spectra are quite similar for each frequency band, except at the frequency of $0.85\, f_{\max}$, where there is a strong tone noise for $I = 8$ deg.

The spectra obtained with SEM (lower plots in Fig. 20) allow us to make the following comments:

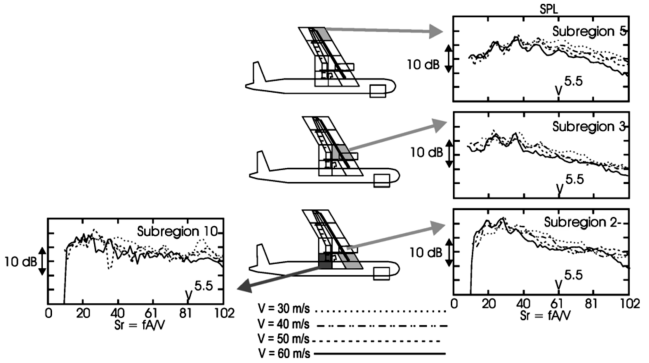

Fig. 19 Flow speed effects: scaled spectra with a speed law in V^{α}, $\alpha = 5.5$. Spectra are presented as a function of the Strouhal number Sr.

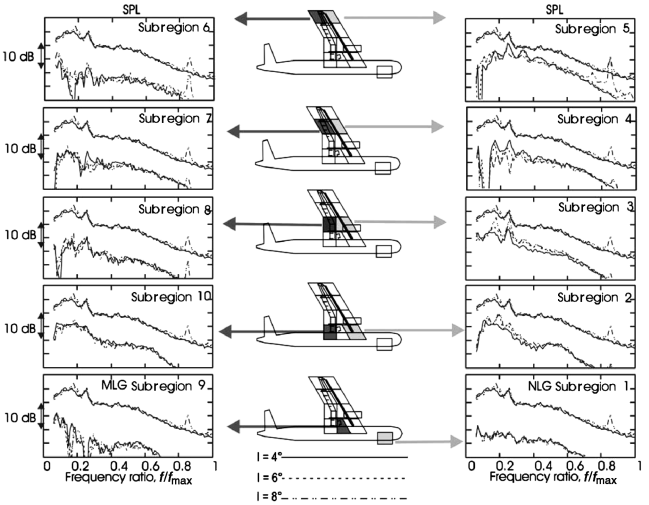

Fig. 20 Effect of the angle of attack: $I = 4$, 6, and 8 deg. Measured spectra are the upper plots and estimated spectra the lower plots.

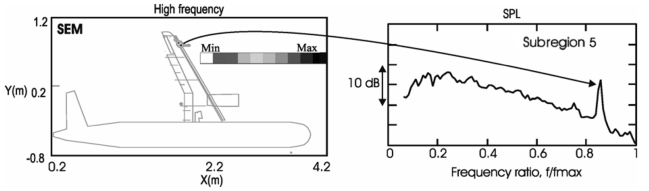

Fig. 21 Localization map at the tone noise frequency and the integrated power levels computed with SEM for subregion 5 located outboard of the wing, for $I = 8$ deg.

1) the noise radiated by the landing gears is not sensitive to changes of the angle of attack;

2) at low frequencies, there is a slight increase in the tone noise level with the angle of attack in the region including the midboard of the slats and the nacelle (subregion 3), and the measurements corroborate this result because an increase in level is also observed with the attack angle at low frequencies;

3) the outboard region of the slats (region 5) is at the origin of the strong tone noise generated for $I = 8$ deg at the frequency of $0.85\, f_{\max}$. Its location is found exactly at the leading edge of the outboard of the slats on the localization map computed with SEM at $f = 0.85\, f_{\max}$ (Fig. 21).

V. Consistency of the SEM Results

In the preceding section, several results were presented concerning the characterization of airframe noise sources, but the accuracy of the data provided by SEM has not been demonstrated. We do not intend in this section to verify this point for all the results examined in the paper. We focus our attention on the examination of the accuracy of the results presented in the previous section concerning the effect of angle of attack.

A. Consistency with Array Data

One first compares the spectra $\Gamma^{\text{mes}}_{18,18}(f)$, measured by microphone 18 of the phased array, to the integrated power levels estimated for the 10 subregions of the complete wing, and for the three values of the angle of attack $I = 4$, 6, and 8 deg, using the following relation:

$$P^{\text{est}}_{n=18}(f) = 10 \log \frac{\sum_{q=1}^{Q} \{ \sum_{j=1}^{N_q} [\alpha_j^2(f)/R_{nj}^2] \}}{p_0^2} \qquad (Q = 10) \quad (8)$$

We can see in Fig. 22 that the integrated power levels for the complete wing are very close to the measured spectra in the whole frequency band considered here. Moreover, the narrowband noise

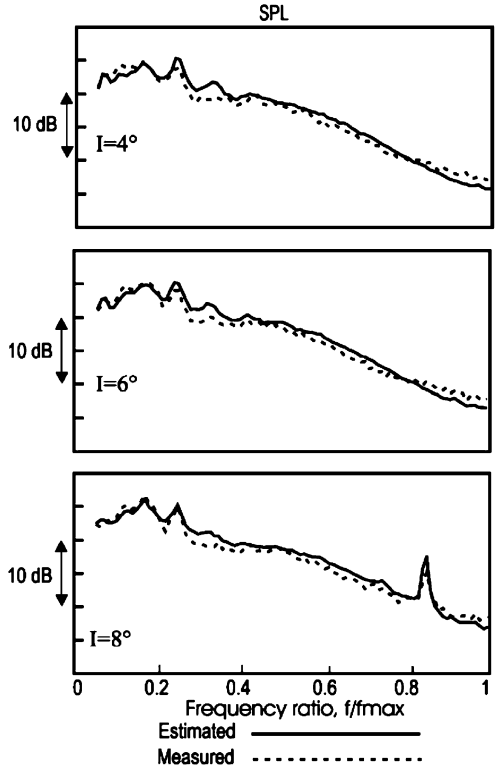

Fig. 22 Comparison of spectra estimated with SEM for the complete wing and spectra measured with the microphone 18 of the array for the configuration examined in Fig. 20 to assess the accuracy of the SEM.

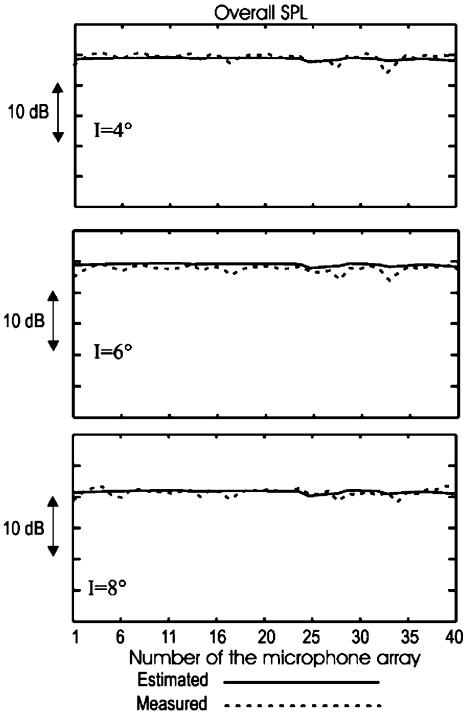

Fig. 23 Comparison of the estimated overall levels with SEM for the complete wing and those measured with the 40 microphones of the phased array for the configuration examined in Fig. 20 to assess the accuracy of the SEM.

and the tone noise measured at low frequencies are well restored by SEM for the three angles of attack. SEM both in terms of frequency and level correctly restored the tone noise measured at high frequencies.

To show that the good match between the estimated and measured spectra obtained for a single microphone does not depend on the choice of the microphone, we now compare $\bar{P}_n^{\text{mes}}(R)$ $(n = 1, 2, \ldots, 40)$ the spectra measured and integrated in the frequency range $[0, f_{\max}]$ for each of the 40 microphones with this relation

$$\bar{P}_n^{\,\text{mes}}(R) = 10 \log \frac{\int_0^{f_{\max}} \Gamma_{n,n}^{\text{mes}}(f)\, \mathrm{d}f}{p_0^2} \tag{9}$$

to $\bar{P}_n^{\text{mod}}(R)$ $(n = 1, 2, \ldots, 40)$ estimated by the SEM for the complete wing with the following expression:

$$\bar{P}_n^{\,\text{mod}}(R) = 10 \log \int_0^{f_{\max}} \frac{\sum_{q=1}^{Q} \{\sum_{j=1}^{N_q} [\alpha_j^2(f)/R_{nj}^2]\}}{p_0^2}\, \mathrm{d}f \tag{10}$$

In Fig. 23 we have plotted $\bar{P}_n^{\text{mod}}(R)$ and $\bar{P}_n^{\text{mes}}(R)$ for $I = 4$, 6, and 8 deg. We can observe the good match between the two curves with slight differences at high frequencies.

B. Consistency with Far-Field Data

One of the main purposes of the power level estimation methods in the study of airframe noise is to identify on the aircraft model, the locations of the noise sources and to estimate their directivity pattern. We have shown that SEM can successfully solve the first part of the problem. Now we give an illustration of the use of SEM in the computation of the spectra radiated in far field by the aircraft model for three azimuthal angles $\theta = 40$, 90, and 140 deg (Fig. 7). The curves presented in Fig. 24 indicate that the integrated power levels for the complete wing obtained using the SEM are reasonably accurate descriptions of the measured spectra. However, we do note a difference of about 5 dB between the two spectra at low frequencies. This is due to the cutoff frequency of the high-pass filter used to reduce the background flow noise on the microphones of the phased array, which is lower than that of the high-pass filter equipping the output of the far-field microphones. One also observes a better accuracy of the spectrum computed underneath the wing $(\theta = 90$ deg), compared to the spectra obtained in the forward $(\theta = 40$ deg) and rearward $(\theta = 140$ deg) directions. We see, in

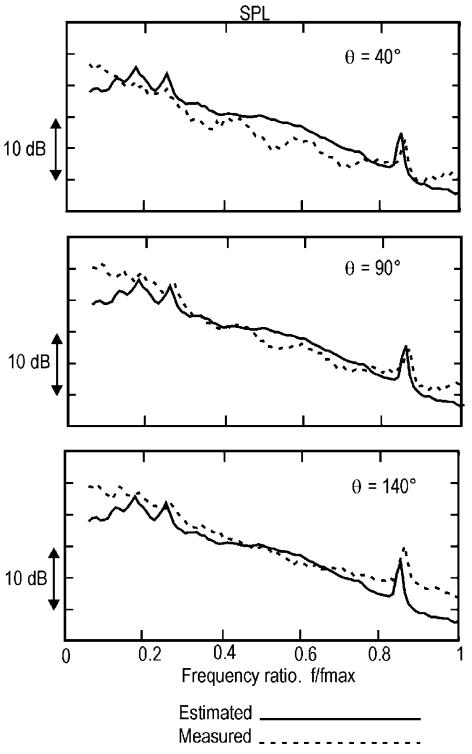

Fig. 24 Application of the SEM: comparison between the far-field spectra measured and estimated with the SEM for the complete wing for three azimuthal angles $\theta = 40$, 90, and 140 deg.

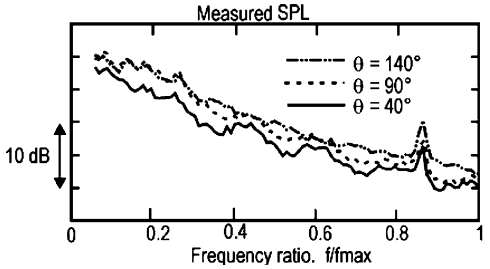

Fig. 25 Comparison between the far-field spectra measured by the microphones at the azimuthal angles $\theta = 40$, 90, and 140 deg.

particular, that there is an underestimation of the source levels at low and medium frequencies for the azimuthal angle 40 deg, and an overestimation at high frequencies for the azimuthal angle 140 deg. We should emphasize that all results computed with SEM were obtained with the data of the cross-shaped array, which measures the noise source radiated directly downward the wing, in the direction of the microphone at 90 deg. In contrast, the microphones at 40 and 140 deg measure the noise characteristics in the forward and rearward directions, respectively, which present some differences compared to the spectra measured in the 90 deg direction as indicated in Fig. 25. This means, in fact, that SEM is able to restore correctly the levels of acoustic source that radiate within the aperture of the array. During the tests, the cross-shaped array was moved in the forward and rearward directions to examine the directivity effects of the noise radiated by the aircraft model. The data recorded for these two directions and used by SEM should improve the accuracy of the results for the forward and rearward directions. In contrast, this solution may fail to work satisfactorily, if there are directivity effects of the acoustic sources radiated by the wing which are not correctly taken into account by the model of uncorrelated monopole sources used in this study. In this situation, we may expect to improve the accuracy of the restoration of the acoustic source levels for the forward and rearward directions by using a model based on a set of correlated monopoles. However, the determination of the amplitude and phase of the correlated monopoles require solving an overdetermined system (i.e., the number of parameters to estimate is much greater than the number of measurements) which leads to biased estimates [17]. At this point, the questions that would be natural to ask are would the errors on the estimates be negligible or would they degrade the quality of the results obtained with a model of uncorrelated monopoles? Further investigations are needed to answer these questions.

VI. Summary

In the first part of the article, the estimation of the power levels of acoustic sources with SEM from phased array measurements was examined.

It has been shown that the absolute levels of broadband sources may be successfully obtained at low frequencies as well as at high frequencies with SEM.

The analysis with SEM of the airframe noise of an Airbus A320/A321 aircraft model tested in the open jet CEPRA 19 wind tunnel has shown the following trends:

1) When the flaps are deployed alone, it was shown that it is mainly broadband noise that dominates at low frequencies from inboard up to midboard leading edge of the flaps and a strong tone noise at high frequencies at the inboard tip of the flaps.

2) When the slats and the flaps are both deployed, it was shown that the noise from the slats predominates on its outboard part, at the junction between the slats and the nacelle. It was also shown that a strong noise source is generated at the wing root.

3) The broadband noise generated by the slats and the flaps is governed by a $V^{6.3}$ and $V^{5.5}$ power scaling law, respectively. In contrast, the tone noise radiated by the slats and the flaps at low frequencies are governed by a Strouhal law and a $V^{5.5}$ power scaling law.

4) It was demonstrated that the increase of the attack angle of the aircraft model has a minor influence on the level of the overall acoustics. We highlighted that for high angles of attack an intense tone noise is produced at the outboard part of the slats.

The accuracy of the experimental results presented in this paper was demonstrated by comparing the spectra measured by the cross-shaped array to the integrated power levels provided by SEM. We also showed the capacity of SEM to correctly restore the far-field spectra of the airframe noise measured within the spatial aperture of the array, and with a slight error, the spectra of the noise sources that radiate outside the aperture.

This study allows us to conclude that SEM is a reliable numerical tool to guide the design of quiet aircraft concepts. The results provided by SEM will be used to constitute an experimental database to improve the understanding of the airframe noise mechanisms.

Acknowledgments

The experiment with the aircraft model was performed under a contract from Airbus Industrie and SPAé (French Service of Aeronautic Programs). The author is grateful to M. M. Georges Élias, Alain Julienne, and Renaud Davy for many stimulating discussions.

References

[1] Oerlemans, S., and Sijtsma, P., "Acoustic Array Measurements of a 1:10.6 Scaled Airbus A340 Model," AIAA Paper 2004-2954, May 2004.

[2] Sodermann, P. T., Kafyeke, F., Burnside, N. J., Chandrasekharan, R., Jaeger, S. M., and Boudreau, J., "Airframe Noise Study of a CRJ-700 Aircraft Model in the NASA AMES 7–by 10–Foot Wind Tunnel No 1," AIAA Paper 2002-2406, June 2002.

[3] Guo, Y. P., and Joshi, M. C., "Noise Characteristics of Aircraft High Lift Systems," *AIAA Journal*, Vol. 41. No. 7, 2003, pp. 1247–1256.

[4] Dobrzynski, W., Chow, L. C., Guion, P., and Shiells, D., "Research into Landing Gear Airframe Noise Reduction," AIAA Paper 2002-2409, June 2002.

[5] Chow, L., Mau, K., and Remy, H., "Landing Gears and High Lift Devices Airframe Noise Research," AIAA Paper 2002-2408, June 2002.

[6] Davy, R., Moens, F., and Rémy, H., "Aeroacoustic Behavior of a 1/11 Scale Airbus Model in the Open Anechoic Wind Tunnel CEPRA 19," AIAA Paper 2002-2412, June 2002.

[7] Élias, G., "Source Localization with a Two-Dimensional Focused Array- Optimal Processing for a Cross-Shaped Array," Inter-Noise, July 1995.

[8] Piet, J. F., and Élias, G., "Airframe Noise Source Localization Using a Microphone Array," AIAA Paper 97-1643, May 1997.

[9] Humphreys, W. M., Brooks, T. F., Hunter, W. W., and Meadows, K. R., " Design and Use of Microphone Directional Arrays for Aeroacoustic Measurements," AIAA Paper 98-0471, Jan. 1998.

[10] Mosher, M., "Phased Arrays for Aeroacoustic Testing: Theoretical Development," AIAA Paper 96-1723, May 1996.

[11] Brooks, T. F., and Humphreys, W. M., "A Deconvolution Approach for the Mapping of Acoustic Sources (DAMAS) Determined from Phased Microphone Arrays," AIAA Paper 2004-2954, May 2004.

[12] Blacodon, D., and Élias, G., "Level Estimation of Extended Acoustic Sources Using a Parametric Method," *Journal of Aircraft*, Vol. 41, No. 6, 2004, pp. 1360–1369.

[13] Dowling, A. P., and Ffowcs Williams, J. E., *Sound and Sources of Sound*, Ellis Horwood Publishers, Chichester, 1983.

[14] Bard, Y., *Nonlinear Parameter Estimation*, Academic Press, New York, 1974.

[15] Candel, S., Guédel, A., and Julienne, A., "Radiation, Refraction and Scattering on Waves in a Shear Flow," AIAA Paper 76-544, July 1976.

[16] Amiet, R. K., "Refraction of Sound by a Shear Layer," *Journal of Sound and Vibration*, Vol. 58, No. 3, 1978, pp. 467–482.

[17] Cadzow, J. A., "High Performance Spectral Estimation—A New ARMA Method," *IEEE Transactions on Acoustics, Speech, and Signal Processing*, Vol. 28, No. 5, 1980, pp. 524–529.